Analysis and Numerical Solution of Stochastic Phase-Field Models of Tumor Growth

Ernesto A. B. F. Lima[a,b], Regina C. Almeida[b], J. Tinsley Oden[a],

[a] *Institute for Computational Engineering and Sciences (ICES), The University of Texas at Austin*
[b] *National Laboratory for Scientific Computing (LNCC), Petrópolis, Brazil*

Abstract

Carcinogenesis, as every biological process, is not purely deterministic since all systems are subject to random perturbations from the environment. In tumor growth models, the values of the parameters are subject to many uncertainties that can arise from experimental variations or due to patient-specific data. The present work is devoted to the development and analysis of numerical methods for the solution of a system of stochastic partial differential equations governing a six-species tumor growth model. The model system simulates the stochastic behavior of cellular and macro cellular events affecting the evolution of avascular cancerous tissue. It is a continuous phase-field model that incorporates several key features in tumor dynamics. A sensitivity analysis is performed in order to identify the more influential parameters. A mixed finite element method and a stochastic collocation scheme are introduced to approximate random-variables components of the solution. The results of numerous numerical experiments are also presented and discussed.

Keywords: Avascular Tumor Growth, Mixture Theory, Stochastic Collocation Method, Finite Element Method

1. Introduction

Tumor environment is composed by many constituents, such as, different types of tumor cells, blood vessels, nutrients, immune system cells, healthy cells, among others. When modeling multiphase materials, such as cancer, one modeling challenger is how to handle interface between phases. Notwithstanding, phase-field or diffuse-interface models provide general approaches in which the interface between constituents is handled naturally as a feature of the solution. In recent years, interest in Cahn-Hillard type equations have received increasing interest because of their ability to model complex phase changes in materials, originating in studies of binary fluids and spinodal decomposition (e.g. [4, 7, 8]). These are nonlinear evolution equations, fourth-order in spatial variables that depict the evolution and motion of interfaces between two phases, or "constituents", as mass or energy is transferred from one species to another. A significant generalization of these models has appeared in recent years in the form of continuum mixture of models of multiple species media, and such models have proved to be well suited for depicting the complex behavior of tumor growth (e.g. [5, 25, 10, 13]). The resulting evolution equations are inherently "stiff", owing to non-convex terms in the total energy of the system, and special methods of numerical time integration must be employed to numerically treat such systems [6, 8, 10, 13].

The Cahn-Hilliard equation provides the basis for the development of a series of tumor growth models [5, 25, 10, 13]. The model developed by Cristini et al. [5] considers the evolution of the nutrient as a reaction-diffusion equation and the mixture, composed by tumor cells and water, is modeled by a phase field equation. As the model does not consider the dead cells as a separate constituent, when the cells inside the tumor die because of the lack of oxygen, water occupies their original position, without representing the characteristic necrotic core. The model developed by Wise et al. [25] also considers the evolution of the nutrient as a reaction-diffusion equation but splits the tumor into viable and dead cells. This modification allows the representation of dead cells inside the tumor due to the lack of nutrients and oxygen. The model developed by Hawkins-Daarud et al. [10] is a four-species tumor growth model, in which the extracellular water is divided into nutrient rich and nutrient poor parts, which are incorporated into the mixture. Although in [10] the nutrient is incorporated as part of the mixture, the model does not reproduce the necrotic core inside

the tumor. A general hybrid ten-species tumor growth model of this general type was recently developed by the authors [13] and it forms a starting point for the present study. In Lima et al. [13], besides tumor cells divided into proliferative, hypoxic (quiescent) and necrotic states, healthy cells, nutrient, tumor growth factor and endothelial cells are all incorporated into the mixture. The local dynamics among the mixture constituents involves phenomena such as self-sufficiency in growth signals, insensitivity to anti-growth signals, programmed cell death and limitless replicative potential through a complex interplay between mortality and natality dynamics. The hypoxic and endothelial cells are strongly linked to the discrete model that describes angiogenesis. While it is well known that tumor metastasis is generally activated by random biological signals originating at a cellular level, and while these processes affect critical proliferation rates that directly influence the growth and decline of tumor cells, general PDE models of tumor growth that account for stochasticity are rare in the literature. The development of such models and their numerical solution is the subject of this work.

The previous models listed mainly consist in deterministic representations of the tumor growth. However, it is widely accepted that tumor growth can be regarded as a random process due to stochastic proliferation and differentiation of cells [24]. When modeling carcinogenesis, variables such as proliferation and apoptosis rates are approximated by data collected *in vitro*, that are intended to reproduce similar conditions *in vivo*. Obviously, these values are subject to many uncertainties. Consequently, to take into account such uncertainties, the carcinogenesis must be modeled as a stochastic process [15].

Several papers can be found in the literature that treat uncertainties in tumor growth [14, 15, 17, 19, 22, 24, 16, 18, 1, 2]. Stochastic angiogenesis models are thought to be able to generate more realistic structures of capillary networks [19]. Liotta et al. [14] developed a stochastic model of metastasis formation, that takes into account the fact that a great number of tumor cells can enter the circulatory system, but less than 0.1% survive to form metastasis. Mortality and natality rates can also be treated as random variables [15, 24]. In Lo [15], the action of various therapies, such as chemotherapy, is modeled, which can be used to model the suppression of growth of tumor. In Naumov et al. [18], a cellular automata model for the tumor growth is developed. In their work the natural shrinkage in tumors is considered a stochastic process. They assume that a cell size is reduced to one-third of its original size under necrosis. In this work, a stochastic rule is used to determine that only one-third of all cells become necrotic and, due to the accompanied shrinkage, the remaining empty space represents the reduction of the tumor size.

Hybrid stochastic models have also been proposed which employ cellular automata models with probabilistic transition rules [17, 22, 16]. In the model proposed by Macklin et al. [16], the cells transition rules from one state to another are stochastic. The probability of a cell entering another state is given by an exponentially-distributed random variable. Quaranta et al. [22] model tumor invasion of surrounding tissue through a partial differential equations and a stochastic cellular automata model (*random-walk model*) to depict cell migration and cell-cell interactions. In Mallet and De Pillis [17], a hybrid cellular automata model combined with a model involving partial differential equations is presented to model the interaction between tumor cells and the immune system. In this model a reaction-diffusion equation is used to describe the distribution of two chemicals necessary for mitosis and cell survival. Among the stochastic processes considered in the cellular automata, the death of tumor cells due to insufficient nutrients and actions of the immune system can be modeled as well as tumor and immune cell division and migration [17].

Here we develop a tumor growth model that accounts for random perturbations that arise from modeling uncertainties in the parameters. To provide focus, we consider an avascular model with six constituents derived directly from the hybrid ten-species model developed in Lima et al. [13]. Since this simplified model still has many parameters, a sensitivity analysis is performed to identify the more influential parameters on the tumor mass growth. The stochastic model is then developed taking into account the uncertainty of the most influential parameter. To the best of the authors knowledge, present study is believed to be the first to explore the use of CH-type systems with uncertain parameters to study the tumor growth through stochastic models.

Following this introduction, we review the models of tumor morphology and key biological mechanisms of tumor growth covered in the deterministic ten-species model of Lima et al. [13], with the simplification that angiogenesis is ignored and, therefore, the evolution of tumor angiogenesis factors (TAF's) are eliminated, resulting in a six-species model. The governing system of evolution equations is presented together with their mixed finite-element approximations. A time-discretization scheme is presented together with a Gauss-Seidel scheme for solving linearizations of the nonlinear systems over a time step.

In section 3 of the paper, we describe a sensitivity analysis of the avascular model, focusing on how uncertainties in model parameters influence model outputs, for a selected set of parameters and outputs. The analysis follows that of Saltelli et al. [23] and employs a straightforward Monte Carlo algorithm leading

to scatterplots of the output, generally depicting the tumor mass at selected times.

In section 4 of the paper, we describe a probabilistic framework leading to a system of stochastic partial differential equations (SSPDE's). We present weak formulations of the systems and describe an implementation of a stochastic collocation algorithm for treating the random components of the dependent variables, a mixed finite element approximation being used for spatial approximations and the time marching algorithms being essentially the same as the deterministic case. The results of several numerical experiments are described. Conclusions of the study are presented in a final section.

2. The avascular model: a six-constituents model

In [13], a deterministic hybrid ten-constituent phase-field model that integrates the continuous description of tumor growth and discrete description of angiogenesis processes is presented. Here we review details of the derivation of such model and describe a stochastic system for a relevant subclass of models. In the hybrid model [13], the interface among constituents is handled naturally as a feature of the solution owing to the phase-field or diffuse-interface framework [21]. The continuous macroscopic model considers a mixture of ten constituents. The solid constituents are represented by healthy cells, proliferative and non-activated endothelial cells, and tumor cells, which are divided into necrotic core and hypoxic and proliferating tumor cells. The fluid constituents are nutrient-rich and nutrient-poor extracellular water, and tumor angiogenesis factor (TAF) -rich and -poor extracellular water. TAF-rich extracellular water is released by hypoxic cells and plays the role of the key regulator of the tumor angiogenesis, modeled by a microscopic agent based model. The discrete model drives the vascular development through tip endothelial cell (tip cell) activation that ultimately activates quiescent endothelial cells, yielding new vessel sprouting.

Here, the avascular counterpart of the hybrid phase-field model [13] is chosen as the basis of the proposed stochastic model. The avascular model is derived directly from [13] by assuming that there is no release of TAF and, consequently, no angiogenesis. In this case, no new blood vessels are created and no new source of nutrients is provided so that the endothelial cells do not play a role on the dynamics of the system. Since there is no TAF, the hypoxic cells could be merged with proliferating cells. However, we choose to maintain all cells stages of the original ten-species model, so that a new mixture emerges with the following six constituent volume fractions:

- ϕ_P - proliferative tumor cell;
- ϕ_H - hypoxic tumor cell;
- ϕ_N - necrotic core;
- ϕ_σ - nutrient-rich extracellular water;
- ϕ_{σ_0} - nutrient-poor extracellular water;
- ϕ_C - healthy cell.

The mixture is assumed to be saturated, which means that $\phi_T+\phi_C+\phi_\sigma+\phi_{\sigma_0}=1$, where $\phi_T=\phi_P+\phi_H+\phi_N$. The solid $s=\phi_T+\phi_C$ and fluid $w=\phi_\sigma+\phi_{\sigma_0}$ volume fractions of the mixture can be rescaled to vary from 0 to 1 depending on a constant C by defining $s=C$ and $w=1-C$. This means that the values of ϕ_T and ϕ_σ are normalized so as to take on values between 0 and 1. The mixture is defined over the bounded domain $\Omega\subset\mathbb{R}^d\,(d=1,2,3)$ with a Lipschitz continuous boundary Γ with an outward unit normal $\boldsymbol{n}$, at the time interval $(0,T)$. Each constituent must satisfy its own balance law given by

$$\left.\begin{aligned}
\frac{\partial\phi_P}{\partial t} &= -\boldsymbol{\nabla}\cdot\boldsymbol{J}_P+S_P,\\
\frac{\partial\phi_H}{\partial t} &= -\boldsymbol{\nabla}\cdot\boldsymbol{J}_H+S_H,\\
\frac{\partial\phi_N}{\partial t} &= -\boldsymbol{\nabla}\cdot\boldsymbol{J}_N+S_N,\\
\frac{\partial\phi_\sigma}{\partial t} &= -\boldsymbol{\nabla}\cdot\boldsymbol{J}_\sigma+S_\sigma,
\end{aligned}\right\} \tag{1}$$

where the mass fluxes are given by

$$\left.\begin{array}{rcl} \boldsymbol{J}_P &=& -M_P \boldsymbol{\nabla} D_{\phi_P} E, \\ \boldsymbol{J}_H &=& -M_H \boldsymbol{\nabla} D_{\phi_H} E, \\ \boldsymbol{J}_N &=& -M_N \boldsymbol{\nabla} D_{\phi_N} E, \\ \boldsymbol{J}_\sigma &=& -M_\sigma \boldsymbol{\nabla} D_{\phi_\sigma} E. \end{array}\right\} \tag{2}$$

Here, M_P and $D_{\phi_P}(\cdot)$ are the mobility of constituent ϕ_P and the functional derivative with respect to ϕ_P, respectively. Similar notation is used for the other constituents. Finally, E stands for the free energy functional, which results from the interactions among each constituent. The tumor cells (proliferative, hypoxic and necrotic) have similar adhesive properties and they prefer to adhere to one another [25], causing a segregation from healthy cells. This behavior of separation among phases, typical of binary Cahn-Hilliard systems, is modeled by a double-well potential and a capillary interfacial energy. The presence of nutrient-rich volume fraction in the mixture contributes to an increase of the system energy through a quadratic term and interferes chemotactically with tumor cells, yielding a directional movement towards nutrient supply [5, 10]. These assumptions yield the following total energy of the system:

$$E = \int_\Omega \left[\Psi(\phi_T) + \frac{\epsilon_T^2}{2} |\boldsymbol{\nabla}\phi_T|^2 + \frac{1}{2\delta_\sigma}\phi_\sigma^2 + \chi\left(\phi_T, \phi_\sigma\right) \right] dx. \tag{3}$$

In this definition, $\delta_\sigma > 0$ is a small parameter and $\chi\left(\phi_T, \phi_\sigma\right) = -\chi_0 \phi_T \phi_\sigma$, where χ_0 is a positive constant governing the relative strength of the interaction among tumor cells and nutrient. The second term in (3) defines the interfacial surface energy due to spatial concentration gradient, where the small parameter ϵ_T is the interaction length. Finally, $\Psi(\phi_T)$ is defined by the quartic double-well function

$$\Psi(\phi_T) = \bar{E}\phi_T^2 \left(1 - \phi_T\right)^2, \tag{4}$$

where $\bar{E} > 0$ is an energy scale.

The mass exchange terms among the mixture constituents are strongly dependent on the nutrient availability provided by the pre-existing blood vessels. Thus, the source terms are obtained by restricting the ones defined in [13] to the avascular case, yielding

$$\left.\begin{array}{rcl} S_P &=& \lambda_P \phi_\sigma \phi_P - \lambda_A \phi_P - \lambda_{PH} \mathscr{H}\left(\sigma_{PH} - \phi_\sigma\right) \phi_P \\ &+& \lambda_{HP} \mathscr{H}\left(\phi_\sigma - \sigma_{HP}\right) \phi_H, \\ S_H &=& -\lambda_A \phi_H + \lambda_{PH} \mathscr{H}\left(\sigma_{PH} - \phi_\sigma\right) \phi_P - \lambda_{HP} \mathscr{H}\left(\phi_\sigma - \sigma_{HP}\right) \phi_H \\ && -\lambda_{HN} \mathscr{H}\left(\sigma_{HN} - \phi_\sigma\right) \phi_H, \\ S_N &=& \lambda_{HN} \mathscr{H}\left(\sigma_{HN} - \phi_\sigma\right) \phi_H, \\ S_\sigma &=& -\lambda_P \phi_\sigma \phi_P - \lambda_{P_h} \phi_\sigma \phi_H + \lambda_A \left(\phi_P + \phi_H\right). \end{array}\right\} \tag{5}$$

As indicated in (5), the proliferating tumor cells is assumed to grow continuously when consuming nutrient with a constant rate of cellular mitosis λ_P. They also decay due to natural death of cells at the apoptosis rate λ_A. Eventually, nutrient intakes become insufficient to maintain their growth, stopping mitosis, so that proliferating tumor cells enter in a hypoxic (quiescent) state. Quiescence is a cell resting state in which it does not proliferate, consumes nutrient at a rate λ_{P_h} and may die by apoptosis, at a rate λ_A. Part of dead cells are degraded for reuse and ultimately increase the nutrient-rich extracellular water volume fraction. The nutrient intakes may continue to drop bellow a certain threshold that can not sustain hypoxia, yielding tumor cells death. This is an unprogrammed cell death called necrosis. Here we consider that necrotic tissue undergoes calcification so that, once formed, a necrotic core never decreases. The nutrient thresholds involved in the transfer from proliferative to hypoxic cell states and from hypoxic to necrotic cell states are denoted by σ_{PH} and σ_{HN}, respectively. These transfers are triggered by using the Heaviside function $\mathscr{H}$, whose value is one for positive arguments and zero otherwise. The vascular tumor model developed in [13] also considers the transfer from hypoxic to proliferative cell states due to an increase of nutrient

availability, mainly due to neovascularization through angiogenesis. This reverse dynamics is kept in the present avascular model, although never activated for the considered model parameters, and is represented by the third term in (5a), where σ_{HP} stands for the nutrient threshold involved in this transfer.

Combining (2) and (3), the system (1) can be rewritten as

$$\left.\begin{aligned}
\frac{\partial \phi_\sigma}{\partial t} &= \boldsymbol{\nabla}\cdot M_\sigma \delta_\sigma^{-1}\boldsymbol{\nabla}\phi_\sigma - \boldsymbol{\nabla}\cdot M_\sigma\chi_0\boldsymbol{\nabla}\phi_T + S_\sigma,\\
\frac{\partial \phi_T}{\partial t} &= \boldsymbol{\nabla}\cdot \mathcal{M}(\phi_T,\phi_H,\phi_N)\boldsymbol{\nabla}\mu + S_T,\\
\mu &= \Psi'(\phi_T) - \epsilon_T^2\Delta\phi_T - \chi_0\phi_\sigma = D_{\phi_T}E,\\
\frac{\partial \phi_H}{\partial t} &= \boldsymbol{\nabla}\cdot \bar{M}_H\phi_H^2\boldsymbol{\nabla}\mu + S_H,\\
\frac{\partial \phi_N}{\partial t} &= \boldsymbol{\nabla}\cdot \bar{M}_N\phi_N^2\boldsymbol{\nabla}\mu + S_N,
\end{aligned}\right\} \text{ in } \Omega\times(0,T), \tag{6}$$

where $S_T = \lambda_P\phi_\sigma\left(\phi_T-\phi_H-\phi_N\right) - \lambda_A\left(\phi_T-\phi_N\right)$. Concentration dependent mobilities are assumed for tumor cells [13] so that $\mathcal{M}(\phi_T,\phi_H,\phi_N) = \bar{M}_P(\phi_T-\phi_H-\phi_N)^2 + \bar{M}_H\phi_H^2 + \bar{M}_N\phi_N^2$, $M_H = \bar{M}_H\phi_H^2$ and $M_N = \bar{M}_N\phi_N^2$, where $\bar{M}_P$, $\bar{M}_H$ and $\bar{M}_N$ are positive constants. Moreover, the first equation in (6) is obtained by substituting $D_{\phi_\sigma}E$ into the flux $\boldsymbol{J}_\sigma = -M_\sigma\boldsymbol{\nabla}D_{\phi_\sigma}E$. By setting the mobility for the nutrient-rich constituent $M_\sigma = \delta_\sigma D$, $D>0$, we notice that the dynamics of the nutrient constituent is simply governed by diffusion, disregarding other interactions. Finally, typical boundary conditions are listed as follows:

$$\left.\begin{aligned}
\boldsymbol{\nabla}\phi_T\cdot\boldsymbol{n} = \boldsymbol{\nabla}\mu\cdot\boldsymbol{n} = \boldsymbol{\nabla}\phi_H\cdot\boldsymbol{n} = \boldsymbol{\nabla}\phi_N\cdot\boldsymbol{n} = 0,\\
\phi_\sigma = 1,
\end{aligned}\right\} \text{ on } \Gamma\times(0,T). \tag{7}$$

2.1. Deterministic problem: numerical approximation

The computational framework to solve the deterministic system (6) is similar to that one developed in [13], which consists of a discrete-time scheme based on the energy convex-nonconvex splitting (see [13] for details). In Eyre [8], unconditionally stable schemes for gradient flows, such as Cahn-Hilliard type problems, are proposed by splitting the energy functional into contractive and expansive terms. The more stable contractive term is treated implicitly and the expansive term explicitly. Although not unique, such splitting always exists for every form of the energy functional and may yield linear schemes. Here we propose $E\left(\phi_T,\phi_\sigma\right) = E_c\left(\phi_T,\phi_\sigma\right) - E_e\left(\phi_T,\phi_\sigma\right)$, where

$$E_c\left(\phi_T,\phi_\sigma\right) = \int_\Omega\left(\frac{3\bar{E}}{2}\phi_T^2 + \frac{\epsilon_T^2}{2}|\boldsymbol{\nabla}\phi_T|^2 - \chi_0\phi_T\phi_\sigma + \frac{\phi_\sigma^2}{2\delta_\sigma}\right)dx, \tag{8}$$

$$-E_e\left(\phi_T,\phi_\sigma\right) = \int_\Omega\left(\bar{E}\left(\phi_T^4 - 2\phi_T^3 - \frac{1}{2}\phi_T^2\right)\right)dx. \tag{9}$$

To define the semi-implicity scheme applied to (6), let the time domain be divided into time steps $\Delta t_n = t_{n+1}-t_n$, $n=0,1,\ldots$, assumed constant for simplicity ($\Delta t_n = \Delta t$). We denote the approximation to $\phi_T^h(t_n)$ by ϕ_{T_n} and likewise to the other variables. Using (8) and (9), and finite difference approximations on

the time derivatives (backward Euler method), the energy convex-nonconvex splitting applied to (6) reads

$$\left.\begin{array}{rcl}
\dfrac{\phi_{\sigma_{n+1}}-\phi_{\sigma_n}}{\Delta t} &=& \boldsymbol{\nabla}\cdot D\boldsymbol{\nabla}\phi_{\sigma_{n+1}} - \boldsymbol{\nabla}\cdot\delta_\sigma D\chi_0\boldsymbol{\nabla}\phi_{T_{n+1}} + S_\sigma(t_{n+1}),\\
\dfrac{\phi_{T_{n+1}}-\phi_{T_n}}{\Delta t} &=& \boldsymbol{\nabla}\cdot\mathcal{M}(\phi_T,\phi_H,\phi_N)|_{n+1}\boldsymbol{\nabla}\mu_{n+1} + S_T(t_{n+1}),\\
\mu_{n+1} &=& D_{\phi_T}E_c\left(\phi_{T_{n+1}},\phi_{\sigma_{n+1}}\right) - D_{\phi_T}E_e\left(\phi_{T_n},\phi_{\sigma_n}\right),\\
\dfrac{\phi_{H_{n+1}}-\phi_{H_n}}{\Delta t} &=& \boldsymbol{\nabla}\cdot\bar{M}_H\phi^2_{H_{n+1}}\boldsymbol{\nabla}\mu_{n+1} + S_H(t_{n+1}),\\
\dfrac{\phi_{N_{n+1}}-\phi_{N_n}}{\Delta t} &=& \boldsymbol{\nabla}\cdot\bar{M}_N\phi^2_{N_{n+1}}\boldsymbol{\nabla}\mu_{n+1} + S_N(t_{n+1}),
\end{array}\right\}\ \text{in } \Omega\times(0,T). \tag{10}$$

We remark that the semi-implicit scheme (10) leads to a huge computational savings owing to the gradient stability property, that allows using greater time-step sizes than other typical schemes [8]. The solution of the highly nonlinear coupled system (10) is accomplished by uncoupling the equations and using an iterative Gauss-Seidel strategy. For clarity, a modification of the algorithm developed in [13] to solve the deterministic nonlinear system is reproduced here. In Algorithm 1, the subscript 0 stands for initial solution, k is the iteration index, *niter* the maximum number of iterations at each time step and *tol* is the tolerance for the iterative process. The iterative loop encompasses the solution of four linear systems and the convergence of the nonlinear solution at each time is achieved with respect to the tumor volume fraction, when $\max|\phi^{k+1}_{T_{n+1}} - \phi^{k}_{T_{n+1}}| < tol$. For the parameter ranges considered here, no more than three iterations are necessary to achieve convergence, yielding remarkable computational savings as compared with the fully coupled solver. The four algebraic systems are obtained by using the Galerkin finite element method. To define the finite element approximation to (10), we assume homogeneous Neumann boundary conditions for all variables for simplicity. Let $\mathcal{V}\equiv H^1(\Omega)$, $\mathcal{V}^h\subset\mathcal{V}$. Then

$$\mathcal{V}^h \;=\; \{v\in C^0(\bar{\Omega})\cap\mathcal{V} : v|_\tau = \bar{v}\circ F_\tau = \bar{v}\in\mathbb{Q}_1, \tau\in\mathcal{T}^h\},$$

where $\mathcal{T}^h$ is a quasi-uniform family of triangulations of Ω, F_τ is an affine map from the master element $\bar{\tau}$ into τ and $\mathbb{Q}_1$ is the tensor product of polynomials of degree 1. Let $\mathcal{V}^h = span\{\psi_i\}$ so that each constituent approximation is built by a linear combination of this basis. Denoting $(\cdot,\cdot)$ as the L^2-inner product over Ω : $(u,v) = \displaystyle\int_\Omega uvdx$, the discrete variational forms are given by: For each k, find ${\phi_T}^{k+1}_{n+1}$, μ^{k+1}_{n+1}, ${\phi_H}^{k+1}_{n+1}$,

${\phi_N}_{n+1}^{k+1}$, ${\phi_{\sigma}}_{n+1}^{k+1} \in \mathcal{V}^h$, $\forall\ \widehat{\phi}_T$, $\widehat{\mu}$, $\widehat{\phi}_H$, $\widehat{\phi}_N$, $\widehat{\phi}_\sigma \in \mathcal{V}^h$, such that:

$$\begin{aligned}
\left(\phi_{\sigma_{n+1}}^{k+1} - \phi_{\sigma_n}, \widehat{\phi}_\sigma\right) &+ \Delta t \left(D \boldsymbol{\nabla} \phi_{\sigma_{n+1}}^{k+1}, \boldsymbol{\nabla} \widehat{\phi}_\sigma\right) \\
&+ \Delta t \lambda_P \left(\left({\phi_T}_{n+1}^{k} - {\phi_H}_{n+1}^{k} - {\phi_N}_{n+1}^{k}\right) \phi_{\sigma_{n+1}}^{k+1}, \widehat{\phi}_\sigma\right) \\
&+ \Delta t \lambda_P \left({\phi_H}_{n+1}^{k} \phi_{\sigma_{n+1}}^{k+1}, \widehat{\phi}_\sigma\right) \\
&= \Delta t \lambda_A \left({\phi_T}_{n+1}^{k} - {\phi_N}_{n+1}^{k}, \widehat{\phi}_\sigma\right) \\
&+ \Delta t \left(\delta_\sigma D \chi_0 \boldsymbol{\nabla} {\phi_T}_{n+1}^{k}, \boldsymbol{\nabla} \widehat{\phi}_\sigma\right); \qquad (11)
\end{aligned}$$

$$\begin{aligned}
\left({\phi_T}_{n+1}^{k+1} - \phi_{T n}, \widehat{\phi}_T\right) &+ \Delta t \left(\mathcal{M}\left({\phi_T}_{n+1}^{k}, {\phi_H}_{n+1}^{k}, {\phi_N}_{n+1}^{k}\right) \boldsymbol{\nabla} \mu_{n+1}^{k+1}, \boldsymbol{\nabla} \widehat{\phi}_T\right) \\
&- \Delta t \lambda_P \left(\phi_{\sigma_{n+1}}^{k+1} \left({\phi_T}_{n+1}^{k+1} - {\phi_H}_{n+1}^{k} - {\phi_N}_{n+1}^{k}\right), \widehat{\phi}_T\right) \\
&+ \Delta t \lambda_A \left({\phi_T}_{n+1}^{k+1} - {\phi_N}_{n+1}^{k}, \widehat{\phi}_T\right) = 0; \qquad (12)
\end{aligned}$$

$$\begin{aligned}
\left(\mu_{n+1}^{k+1}, \widehat{\mu}\right) &- \left(D_{\phi_T} E_c \left({\phi_T}_{n+1}^{k+1}, \phi_{\sigma_{n+1}}^{k+1}\right), \widehat{\mu}\right) \\
&= -\left(D_{\phi_T} E_e \left(\phi_{T n}, \phi_{\sigma_n}\right), \widehat{\mu}\right); \qquad (13)
\end{aligned}$$

$$\begin{aligned}
\left({\phi_H}_{n+1}^{k+1} - \phi_{H n}, \widehat{\phi}_H\right) &+ \Delta t \left(\bar{M}_H \left({\phi_H}_{n+1}^{k}\right)^2 \boldsymbol{\nabla} \mu_{n+1}^{k+1}, \boldsymbol{\nabla} \widehat{\phi}_H\right) \\
&+ \Delta t \lambda_A \left({\phi_H}_{n+1}^{k+1}, \widehat{\phi}_H\right) \\
&- \Delta t \lambda_{HP} \left(\mathscr{H}\left(\phi_{\sigma_{n+1}}^{k+1} - \sigma_{HP}\right) {\phi_H}_{n+1}^{k+1}, \widehat{\phi}_H\right) \\
&+ \Delta t \lambda_{PH} \left(\mathscr{H}\left(\sigma_{PH} - \phi_{\sigma_{n+1}}^{k+1}\right) \left({\phi_T}_{n+1}^{k+1} - {\phi_H}_{n+1}^{k+1} - {\phi_N}_{n+1}^{k}\right), \widehat{\phi}_H\right) \\
&+ \Delta t \lambda_N \left(\mathscr{H}\left(\sigma_N - \phi_{\sigma_{n+1}}^{k+1}\right) {\phi_H}_{n+1}^{k+1}, \widehat{\phi}_H\right) = 0; \qquad (14)
\end{aligned}$$

$$\begin{aligned}
\left({\phi_N}_{n+1}^{k+1} - \phi_{N n}, \widehat{\phi}_N\right) &+ \Delta t \left(\bar{M}_N \left({\phi_N}_{n+1}^{k}\right)^2 \boldsymbol{\nabla} \mu_{n+1}^{k+1}, \boldsymbol{\nabla} \widehat{\phi}_N\right) \\
&- \Delta t \lambda_{HN} \left(\mathscr{H}\left(\sigma_{HN} - \phi_{\sigma_{n+1}}^{k+1}\right) {\phi_H}_{n+1}^{k+1}, \widehat{\phi}_N\right) = 0. \qquad (15)
\end{aligned}$$

Herein, the functional derivatives are

$$\begin{aligned}
D_{\phi_T} E_c \left(\phi_T, \phi_\sigma\right) &= 3\bar{E}\phi_T - \epsilon_T^2 \Delta \phi_T - \chi_0 \phi_\sigma, \qquad (16) \\
-D_{\phi_T} E_e \left(\phi_T, \phi_\sigma\right) &= \bar{E}\left(4\phi_T^3 - 6\phi_T^2 - \phi_T\right). \qquad (17)
\end{aligned}$$

Algorithm 1: Algorithm to solve the deterministic nonlinear system (10).

Input: $\phi_{T_0}, \phi_{H_0}, \phi_{N_0}, \phi_{\sigma_0}$, Δt, $niter$, T
Output: $\phi_{T_n}, \mu_n, \phi_{\sigma_n}, \phi_{H_n}, \phi_{N_n}$, $\forall n$
begin
  $n \leftarrow 0$
  repeat
    $\phi^0_{T_{n+1}} \leftarrow \phi_{T_n}, \phi^0_{N_{n+1}} \leftarrow \phi_{N_n}, \phi^0_{H_{n+1}} \leftarrow \phi_{H_n}$
    for $k \leftarrow 1$ **to** $niter$ **do**
      $\phi^k_{T_{n+1}} \leftarrow \phi^{k-1}_{T_{n+1}}, \phi^k_{N_{n+1}} \leftarrow \phi^{k-1}_{N_{n+1}}, \phi^k_{H_{n+1}} \leftarrow \phi^{k-1}_{H_{n+1}}$
      solve $\boldsymbol{\phi^{k+1}_{\sigma_{n+1}}}$ **using (11), given** $\phi_{\sigma_n}, \phi^k_{T_{n+1}}, \phi^k_{N_{n+1}}$
      solve $\boldsymbol{\phi^{k+1}_{T_{n+1}}, \mu^{k+1}_{n+1}}$ **using (12) and (13), given** $\phi_{T_n}, \phi^k_{T_{n+1}}, \phi^k_{H_{n+1}}, \phi^k_{N_{n+1}}, \boldsymbol{\phi^{k+1}_{\sigma_{n+1}}}$
      solve $\boldsymbol{\phi^{k+1}_{H_{n+1}}}$ **using (14), given** $\phi_{H_n}, \phi^k_{H_{n+1}}, \phi^k_{N_{n+1}}, \boldsymbol{\phi^{k+1}_{T_{n+1}}, \mu^{k+1}_{n+1}, \phi^{k+1}_{\sigma_{n+1}}}$
      solve $\boldsymbol{\phi^{k+1}_{N_{n+1}}}$ **using (15), given** $\phi_{N_n}, \phi^k_{N_{n+1}}, \boldsymbol{\phi^{k+1}_{H_{n+1}}, \mu^{k+1}_{n+1}, \phi^{k+1}_{\sigma_{n+1}}}$
      if $\max|\phi^{k+1}_{T_{n+1}} - \phi^k_{T_{n+1}}| < tol1$ **then**
        Stop
      end if
    end for
    $\phi_{T_{n+1}} \leftarrow \phi^{k+1}_{T_{n+1}}, \mu_{n+1} \leftarrow \mu^{k+1}_{n+1}, \phi_{\sigma_{n+1}} \leftarrow \phi^{k+1}_{\sigma_{n+1}}$
    $\phi_{H_{n+1}} \leftarrow \phi^{k+1}_{H_{n+1}}, \phi_{N_{n+1}} \leftarrow \phi^{k+1}_{N_{n+1}}$
    $n \leftarrow n + 1$
  until $n\Delta t > T$;
end

3. Sensitivity Analysis of the Avascular Model

In this section we explore how uncertainty in some input parameters of the deterministic avascular model (6) influence the uncertainty in certain model output, i.e., some quantity of interest (QoI) of the model. Among all the model parameters, we select the six believed to be the cause of relevant variations in the QoI based on previous numerical experiments. Such selection is done judiciously in order to avoid increased complexity, since previous experiments indicated that a wider set of parameters would not increase the variance of the output. Moreover, all other types of information, such as initial and boundary conditions, the physical domain, discretization parameters, are also disregard, i.e. they are not allowed to vary. The methodology used here is inspired by that of Saltelli et al. [23]: the uncertainty analysis is performed through a Monte Carlo analysis and the sensitivity analysis is performed by producing scatterplots. This methodology is detailed as follows.

The uncertainty analysis performed here aims at indentifying the parameters most influential of the evolution of the total tumor mass, the selected QoI denoted by y_T. The relevant inputs in this analysis are the proliferative cells mobility ($\bar{M}_P$), hypoxic cells mobility ($\bar{M}_H$), nutrient mobility (D), rate of proliferative cellular mitosis (λ_P), nutrient consumption coefficient by hypoxic cell (λ_{Ph}) and the chemotactic constant (χ_0). For simplicity, these quantities are assumed to be independent of each other and, in the absence of experimental data, to have a continuous uniform distribution. More precisely, given a parameter α_i, $i = 1, \ldots, 6$, $\alpha_i \sim \mathcal{U}(0.8\bar{\alpha}_i, 1.2\bar{\alpha}_i)$, where $\bar{\alpha}_i$ is the parameter value indicated in Table 1. In this analysis, the range defined by a standard variation of 20% is assumed to be appropriate for all parameter $\alpha_i, i = 1, \ldots, 6$.

We begin the uncertainty analysis by drawing a sample from the respective parameters distributions in order to produce a set of vectors $(\bar{M}_P^{(i)}, \bar{M}_H^{(i)}, D^{(i)}, {\lambda_P}^{(i)}, {\lambda_{Ph}}^{(i)}, {\chi_0}^{(i)})$, $i = 1, \ldots, \mathcal{N}$. Here, $\mathcal{N}$ is the dimension of the Monte Carlo experiment. We then obtain the matrix,

$$\boldsymbol{M} = \begin{bmatrix} \bar{M}_P^{(1)} & \bar{M}_H^{(1)} & D^{(1)} & {\lambda_P}^{(1)} & {\lambda_{Ph}}^{(1)} & {\chi_0}^{(1)} \\ \bar{M}_P^{(2)} & \bar{M}_H^{(2)} & D^{(2)} & {\lambda_P}^{(2)} & {\lambda_{Ph}}^{(2)} & {\chi_0}^{(2)} \\ \bar{M}_P^{(3)} & \bar{M}_H^{(3)} & D^{(3)} & {\lambda_P}^{(3)} & {\lambda_{Ph}}^{(3)} & {\chi_0}^{(3)} \\ \vdots & \vdots & \vdots & \vdots & \vdots & \vdots \\ \bar{M}_P^{(\mathcal{N})} & \bar{M}_H^{(\mathcal{N})} & D^{(\mathcal{N})} & {\lambda_P}^{(\mathcal{N})} & {\lambda_{Ph}}^{(\mathcal{N})} & {\chi_0}^{(\mathcal{N})} \end{bmatrix}, \tag{18}$$

in which each row is a set of parameters used for a single deterministic simulation of the model. Therefore, for a given time of the i^{th} simulation, $i = 1, \ldots, \mathcal{N}$, we may evaluate the corresponding total tumor mass $y_T^{(i)}$. Thus, by conducting separate analyses in time, one may get information on the evolution of the tumor mass over time. This can lead to a high level of redundancy because of the strong relationship between responses from one time to the next. Alternatively, the analysis can be performed at some pre-defined times of the tumor evolution according to some specific feature of the dynamics [11]. Thus, at the end of the uncertainty analysis, the corresponding sets of $\mathcal{N}$ values of the QoI at each desired time t_k are produced, i.e.,

$$\boldsymbol{Y}_{|t_k} = \begin{bmatrix} {y_T}^{(1)} \\ {y_T}^{(2)} \\ {y_T}^{(3)} \\ \vdots \\ {y_T}^{(\mathcal{N})} \end{bmatrix}_{|t_k} . \tag{19}$$

A variety of types of information can be obtained from this uncertainty analysis such as the QoI average, its standard deviation or any other statistic. To identify the most influential parameter for these quantities, the sensitivity analysis is performed here through scatterplots as they provide a simple and informative way for identifying the most influential parameter through visual inspection. This approach is quite simple when dealing with only six input parameters. In other situations, such as when dealing with many input parameters, this can pose some difficulties and other sensitivity analysis techniques may be more appropriate (see [23]). The scatterplots are produced by projecting the $\mathcal{N}$ values of the selected QoI $\boldsymbol{Y}$ against the values of each column of $\boldsymbol{M}$, i.e., against the $\mathcal{N}$ sampled values of each α_i. Each diagram resulting from this projection yields a different pattern created by clouds of points over the range of the uncertain parameter on the abscissa. A more uniform pattern indicates that the parameter plays a lesser role on the QoI while a more defined shape indicates higher correlation or higher influence of the parameter.

3.1. Numerical experiment

As a typical numerical experiment, consider the domain $\Omega = [0, 25.6]^2$ and suppose that the initial tumor subdomain is of the following ellipsoidal shape [5, 10]:

$$\left\{ (x, y) : \frac{(x - 12.8)^2}{2.1} + \frac{(y - 12.8)^2}{1.9} \leq 1 \right\}. \tag{20}$$

It is assumed that there are plenty of nutrients available so that the initial nutrient volume fraction is set equal to 1 over the domain and the boundary conditions are given by (7). Spatial and temporal accuracy are obtained by using a quadrilateral mesh with 1600 uniform elements and $\Delta t = 0.01$. Here, we simulate the tumor growth in the time domain $(0, 20]$ and we pre-define two intermediate times, $t_1 = 5$ and $t_2 = 10$, to perform the analysis. Some numerical experiments indicate that these times are potentially interesting to look at and to appropriately identify interesting features of the tumor growth dynamics. We clarify these choices later. We conduct $\mathcal{N} = 300$ simulation runs that are proven to be enough to provide reasonable scatterplots shapes. Figures 1 and 2 show the scatterplots for $t_1 = 5$ and $t_2 = 10$, respectively. Clearly, the scatterplots show that y_T is more sensitive to the rate of proliferative cellular mitosis λ_P than it is to the nutrient mobility. For all the other parameters, the ordering by their influence on y_T is less clear. Despite slight differences on the cloud patterns, all the other parameters are almost equally less important. This behavior is observed at the two pre-defined times. However, the influence strength of the parameters varies in time: notice that the influence of λ_P is higher at $t_1 = 5$ while the effect of nutrient mobility is stronger at $t_2 = 10$. In summary, the sensitivity analysis shows that the mass of the tumor simulated by the avascular model is more sensitive to the rate of proliferative cellular mitosis and the nutrient mobility than to the other parameters. In the following, we take into account the uncertainty of the rate of proliferative cellular mitosis and investigate their propagation in the avascular stochastic tumor model.

4. Stochastic Avascular Tumor Growth Model

In this section, we investigate the effects of uncertain input parameters in the avascular tumor growth model (6). The uncertainty arises from the rate of proliferative cellular mitosis, which is the most influential parameter on the total tumor mass. Thus, we focus on the system (6) which depends on $\lambda_P(\boldsymbol{x}, t, z)$ with

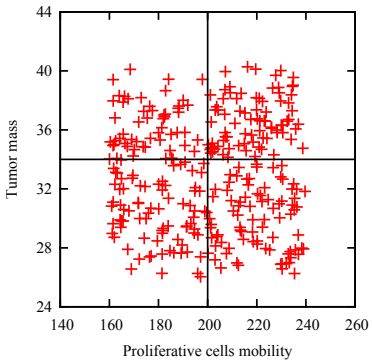

(a) Proliferative cells mobility

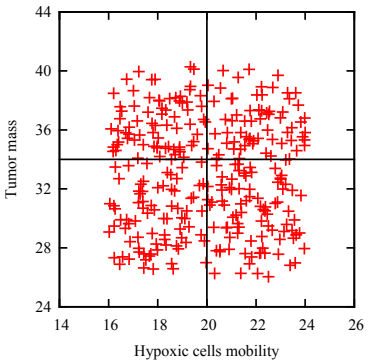

(b) Hypoxic cells mobility

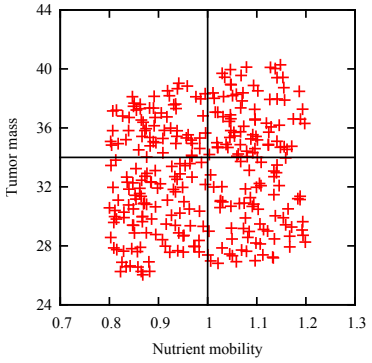

(c) Nutrient mobility

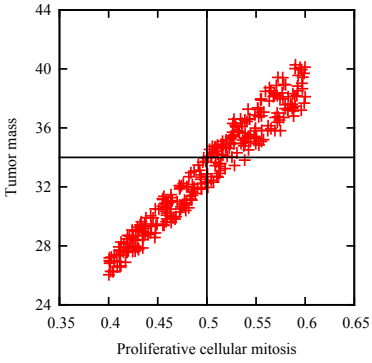

(d) Rate of proliferative cellular mitosis

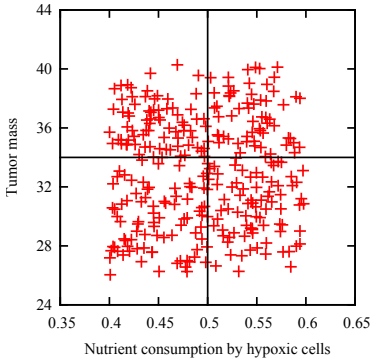

(e) Nutrient consumption coefficient by hypoxic cells

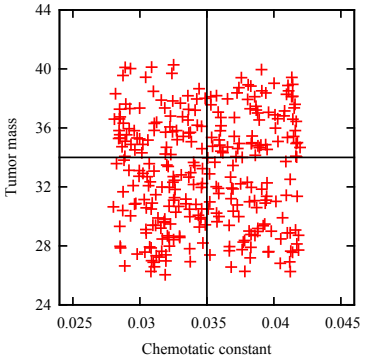

(f) Chemotatic response

Figure 1: Scatterplots of tumor mass versus parameters at time $t_1 = 5$.

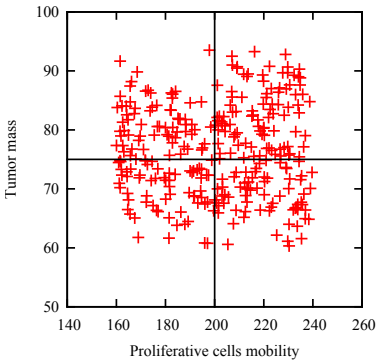

(a) Proliferative cells mobility

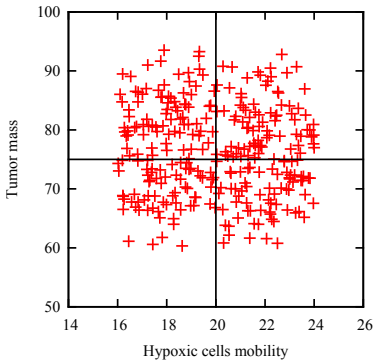

(b) Hypoxic cells mobility

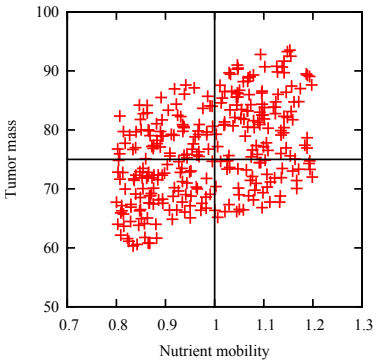

(c) Nutrient mobility

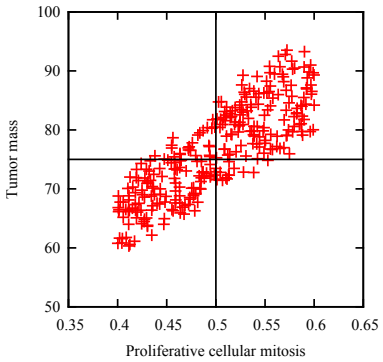

(d) Rate of proliferative cellular mitosis

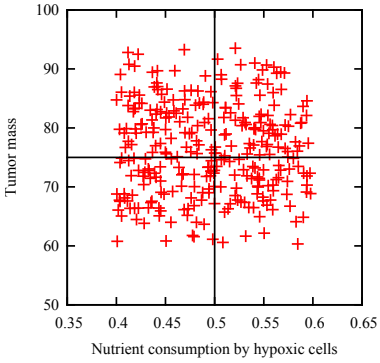

(e) Nutrient consumption coefficient by hypoxic cells

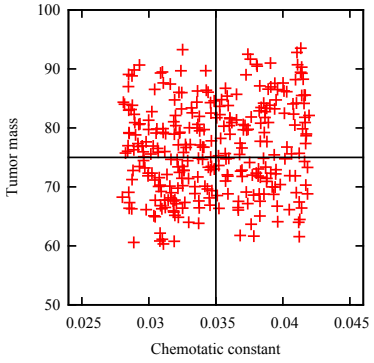

(f) Chemotatic response

Figure 2: Scatterplots of tumor mass versus parameters at time $t_2 = 10$.

$\boldsymbol{x} \in \Omega$, $t \in (0,T]$, $z \in \Upsilon$, where $(\Upsilon, \boldsymbol{U}, \mathbb{P})$ is a complete probability space. Here Υ is the set of outcomes z, $\boldsymbol{U}$ is the σ-algebra of events, and $\mathbb{P} : \boldsymbol{U} \to [0,1]$ a probability measure.

The avascular model (6), in the presence of a random rate of proliferative cellular mitosis, becomes a system of stochastic partial differential equations (SSPDE) defined in $\Omega \times (0,T] \times \Upsilon$, equipped with appropriate boundary and initial conditions. To approach this problem, we consider stochastic processes which can be modeled as second-order random parameters [20], which implies that the randomness is viewed as an additional dimension. For simplicity, we assume that λ_P is constant in the physical space and in time. Thus, the solution of the SSPDE can be described by independent random variables $Y_i(z)$ with pdf $\rho_i : \Sigma^i \to \mathbb{R}$ with bounded ranges Σ^i [20]. The joint probability density is then given by

$$\rho(\boldsymbol{Y}) = \prod_{i=1}^{N} \rho_i(Y_i), \quad \forall \boldsymbol{Y} \in \Sigma, \quad \text{where} \quad \Sigma = \prod_{i=1}^{N} \Sigma^i \subset \mathbb{R}^N. \tag{21}$$

Since N and d are the dimensionality of the truncated random space Σ and the physical space Ω, respectively, the SSPDE is written in $(N+d)$ dimensions as

$$\left.\begin{array}{rcl} \dfrac{\partial \phi_\sigma}{\partial t} &=& \boldsymbol{\nabla} \cdot D \boldsymbol{\nabla} \phi_\sigma - \boldsymbol{\nabla} \cdot \delta_\sigma D \chi_0 \boldsymbol{\nabla} \phi_T + S_\sigma, \\ \dfrac{\partial \phi_T}{\partial t} &=& \boldsymbol{\nabla} \cdot \mathcal{M}(\phi_T, \phi_H, \phi_N) \boldsymbol{\nabla} \mu + S_T, \\ \mu &=& \Psi'(\phi_T) - \epsilon_T^2 \Delta \phi_T - \chi_0 \phi_\sigma = D_{\phi_T} E, \\ \dfrac{\partial \phi_H}{\partial t} &=& \boldsymbol{\nabla} \cdot \bar{M}_H \phi_H^2 \boldsymbol{\nabla} \mu + S_H, \\ \dfrac{\partial \phi_N}{\partial t} &=& \boldsymbol{\nabla} \cdot \bar{M}_N \phi_N^2 \boldsymbol{\nabla} \mu + S_N \end{array}\right\} \text{in } \Omega \times (0,T] \times \Sigma. \tag{22}$$

A more compact representation of the system is given by

$$\mathcal{L}(\boldsymbol{\phi}; \boldsymbol{x}, t, \boldsymbol{Y}) = \mathcal{S}(\boldsymbol{x}, t, \boldsymbol{Y}), \forall (\boldsymbol{x}, t, \boldsymbol{Y}) \in \Omega \times (0,T] \times \Sigma, \tag{23}$$

where $\boldsymbol{\phi}$ is the vector of unknowns $(\phi_T, \mu, \phi_H, \phi_N, \phi_\sigma)$. Let X be an appropriate Hilbert space and $Z \subset L^2_{\mathbb{P}}(\Sigma)$, where

$$\begin{array}{rcl} L^2_{\mathbb{P}}(\Upsilon; W(\Omega)) &=& \{ v : \Upsilon \to W(\Omega) \mid v \text{ is strongly measurable and} \\ && \displaystyle\int_\Upsilon \| v(\cdot, z) \|^2_{W(\Omega)} \, d\mathbb{P}(\Upsilon) < \infty \Big\}. \end{array}$$

The Galerkin weak formulation to (22) reads: for a.e. $(0,T]$, find $\boldsymbol{\phi}(\boldsymbol{x}, t, \boldsymbol{Y}) \in X \times Z$ such that

$$\begin{array}{l} \displaystyle\int_\Sigma \int_\Omega \mathcal{L}(\boldsymbol{\phi}; \boldsymbol{x}, t, \boldsymbol{Y}) \, \boldsymbol{v}(\boldsymbol{x}, \boldsymbol{Y}) \, \rho(\boldsymbol{Y}) \, d\boldsymbol{x} d\boldsymbol{Y} \\ = \displaystyle\int_\Sigma \int_\Omega \mathcal{S}(\boldsymbol{\phi}; \boldsymbol{x}, t, \boldsymbol{Y}) \, \boldsymbol{v}(\boldsymbol{x}, \boldsymbol{Y}) \, \rho(\boldsymbol{Y}) \, d\boldsymbol{x} d\boldsymbol{Y}, \quad \forall \boldsymbol{v}(\boldsymbol{x}, \boldsymbol{Y}) \in X \times Z. \end{array} \tag{24}$$

If $\mathbb{E}[\cdot]$ denotes the expected value, the previous weak formulation may be rewritten as

$$\mathbb{E}\left[\int_\Omega \mathcal{L}(\boldsymbol{\phi}; \boldsymbol{x}, t, \boldsymbol{Y}) \, \boldsymbol{v}(\boldsymbol{x}, \boldsymbol{Y}) \, d\boldsymbol{x} - \int_\Omega \mathcal{S}(\boldsymbol{\phi}; \boldsymbol{x}, t, \boldsymbol{Y}) \, \boldsymbol{v}(\boldsymbol{x}, \boldsymbol{Y}) \, d\boldsymbol{x} \right] = 0. \tag{25}$$

A wide variety of finite element methods can be used to solve stochastic models of this form. The most used techniques are based on the Monte-Carlo (MC) method, generalized Polynomial Chaos (gPC), and the Stochastic Collocation (SC) method. The classical Monte-Carlo method is based on random sampling of the stochastic variable and using these data as input for the deterministic solver, which allows estimating the statistics of the solution [9, 12]. Due to the ease of implementation, it is a popular choice, not requiring changes in the existing deterministic codes, being a non-intrusive method [9, 12, 26]. Although MC methods are conceptually simple, they often cannot be applied in all situations since the convergence generally demands a huge number of realizations [12].

The gPC is a generalization of classical Polynomial Chaos (PC) [26]. In the PC method the stochastic

processes are represented by a Hermite basis, that provides optimal convergence rates for Gaussian processes [26]. In gPC, other orthogonal polynomials are chosen to achieve better convergence for non-Gaussian processes [26]. While delivering faster convergence rates than MC, gPC is a highly intrusive method, requiring a complete change of the deterministic code. Furthermore, the explicit derivation of the gPC equations can be nontrivial, particularly for nonlinear problems [26].

Like MC methods, the Stochastic Collocation (SC) method is non-intrusive, basically involving a deterministic sampling [26]. The deterministic code is employed to find the result for each specific set of samples; after that, the stochastic solution can be estimated. Since it is a deterministic sampling method using a specific set of points in the random space, the computational cost is much lower than MC. Considering the ease of implementation of SC methods as compared to intrusive gPCs and the time-consuming deterministic problem we are dealing with, we use the SC method to solve (23) The detailed description of this methodology and the choice of the collocation points can be found in [12, 26].

The SC method is based on (Lagrange) polynomials interpolation theory in multidimensional random space and on selecting the interpolation points equal to the cubature points. Given a set of distinct collocation points $\Theta_M = \{Z^{(j)}\}_{j=1}^{M} \subset \Sigma_Z \subset \mathbb{R}^N$, where $M \geq 1$ is the number of nodes, the stochastic collocation method is equivalent to solving a deterministic problem at each node $Z^{(j)}$, i.e.,

$$\mathcal{L}\left(\boldsymbol{\phi}; \boldsymbol{x}, t, Z^{(j)}\right) = \mathcal{S}(\boldsymbol{\phi}; \boldsymbol{x}, t, Z^{(j)}), \forall (\boldsymbol{x}, t) \in \Omega \times (0, T]\,. \tag{26}$$

Problem (26) is deterministic since the random parameter is fixed for each $j = 1, \ldots, M$. Thus, the method consists in solving M times the deterministic problem (26) yielding an ensemble of M deterministic solutions $\boldsymbol{\phi}_h^j = \boldsymbol{\phi}_h\left(\boldsymbol{x}, t, Z^{(j)}\right)$. More precisely, the deterministic system (6) is solved for each $\lambda_P = Z^{(j)}$, $j = 1, \ldots, M$, according with Algorithm 1. Once these numerical deterministic solutions are obtained at all collocation points $Z^{(j)}$, $j = 1, \ldots, M$, the mean solution and the variance are computed according to

$$\mathbb{E}[\phi_i] = \sum_{j=1}^{M} \phi_{i_h}(\boldsymbol{x}, t, Z^{(j)})\omega_j,\ var(\phi_i) = \mathbb{E}[\phi_i^2] - (\mathbb{E}[\phi_i])^2, \tag{27}$$

where $\{\omega_j\}$ are the weights associated with the cubature rule and ϕ_i is some constituent volume fraction.

5. Numerical Experiments

Here, we describe the results of numerical experiments designed to evaluate the propagation of uncertainty in the rate of proliferative cellular mitosis and its effect on the dynamics of the avascular tumor growth. The rate of proliferative cellular mitosis is defined as

$$\lambda_P = \bar{\mathcal{P}} + \nu\gamma, \tag{28}$$

where $\bar{\mathcal{P}}$ is the mean value for the proliferation rate, ν the variance chosen such that $\nu < \bar{\mathcal{P}}$ and $\gamma \sim \mathcal{U}[-1, 1]$. The other parameters used for the following numerical simulations are estimated from a variety of sources as indicated in Table 1 (see appendix). The selection of nodes in the stochastic collocation method is a key ingredient in the overall methodology efficiency. The nested Clenshaw-Curtis cubature rule is used, which is proved to be appropriate for a moderate number of random variables [20, 26].

The first experiment is performed under the same conditions of that one in section 3.1. We consider the uncertainty in the rate of proliferative cellular mitosis λ_P, which is set to equal the nutrient consumption coefficient by hypoxic cells, i.e., $\lambda_{P_h} = \lambda_P$. We first run a series of experiments aimed at identifying the level of the cubature rule l to be used in the simulation. The goal is to determine the lower level l to guarantee the desired accuracy. The prescribed accuracy is obtained from the tumor volume fraction and is defined as

$$error = \left\|(\phi_T)_{l-1} - (\phi_T)_l\right\|_\infty \leq 10^{-4}. \tag{29}$$

Figure 3 depicts the error obtained for different interpolation levels. Notice that the pre-defined accuracy is obtained at level $l = 5$, which amounts to using $M = 33$ collocation points. Thus, in the next experiments a Clenshaw-Curtis rule is used with 33 points.

The next experiment compares the evolution of the total tumor mass with two limiting cases corresponding to the Worst-Case Scenarios for the rate of proliferative cellular mitosis. Such limiting cases are obtained

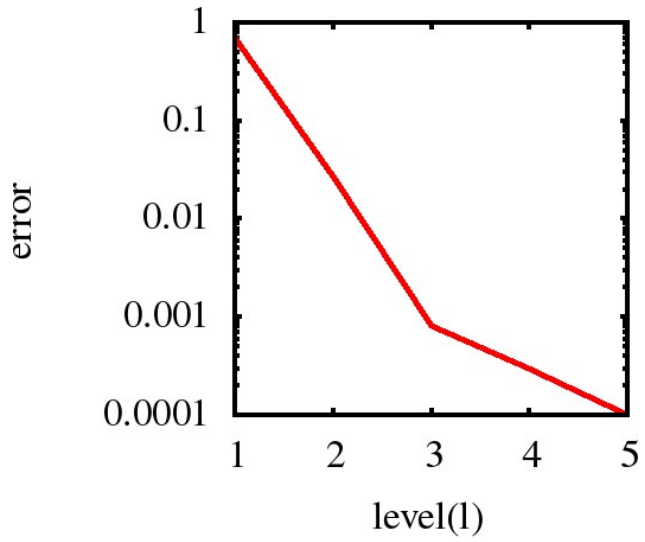

Figure 3: Error for different interpolation levels.

by considering the lower and upper bounds of the random variable, represented by $\gamma = -1$ and $\gamma = 1$. Figure 4(a) shows the mean value for the total tumor mass obtained with the Stochastic Collocation method (in red) and with the Worst-Case Scenarios (in blue). We notice that the tumor grows only until there are enough nutrients. At the beginning of the process, the growth is exponential, but is reduced afterwards due to the decrease of nutrient availability. Due to this limitation, the variance of the tumor mass, depicted in Figure 4(b), is zero at the beginning and at the end of the simulation. The higher variance value occurs at $t = 10.5$, which corresponds to a change of the rate of the total tumor mass. For this reason, the sensitivity analysis was performed at $t = 5$ and $t = 10$, as shown previously through the scatterplots exhibited in Figures 1 and 2, respectively. The higher variance value at $t = 10$ than at $t = 5$ explains the higher dispersion in the scatterplot depicted in Figure 2(d) compared to that in Figure 1(d).

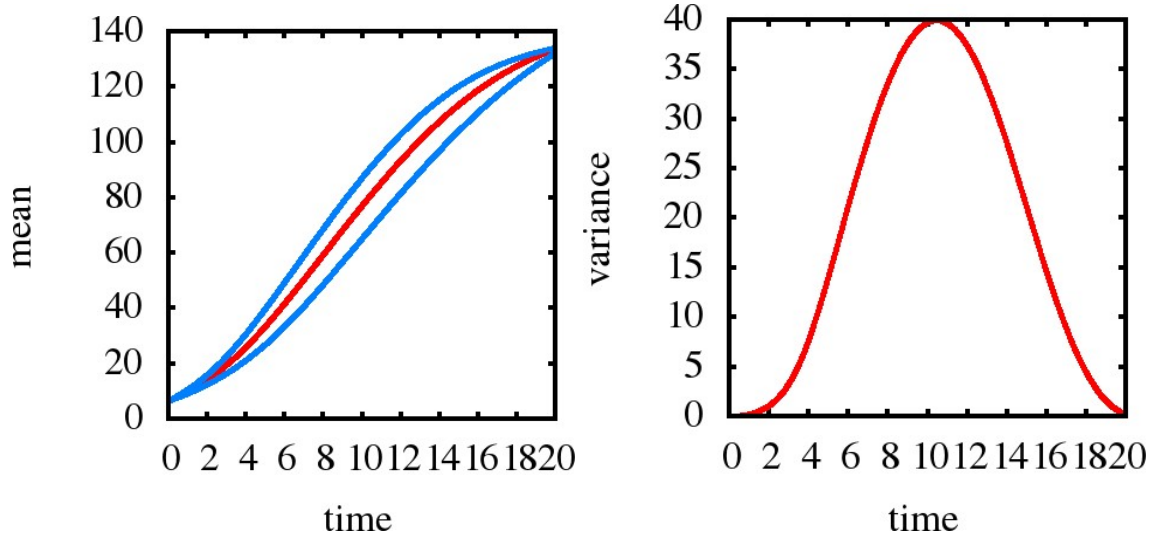

(a) Mass of tumor cells (mean)

(b) Variance

Figure 4: Left: mass of the tumor for the Stochastic Collocation method in red and in blue the Worst-Case Scenario. Right: the variance for the mass of the tumor using the Stochastic Collocation method.

Figure 5 shows the mean and variance for the tumor, hypoxic and necrotic cells and nutrient-rich extracellular water for the random rate of proliferative cellular mitosis. The higher variance of the tumor cells is concentrated mainly on the diffusive interface of the tumor, where the velocity of the tumor growth changes and where there is more proliferative cells. Similar behavior is observed in the variance of the nutrient volume fraction, although there is a decay towards the tumor core due to the presence of hypoxic cells. Finally,

in Figure 6, we compare the shapes of the tumor due to the random proliferative cellular mitosis (in yellow) and due to the Worst-Case Scenarios (in red when $\gamma = 1$ and in green when $\gamma = -1$). For $\gamma = 1$ the shape of the tumor is not radially symmetric while the symmetry if observed for $\gamma = -1$ and the random parameter.

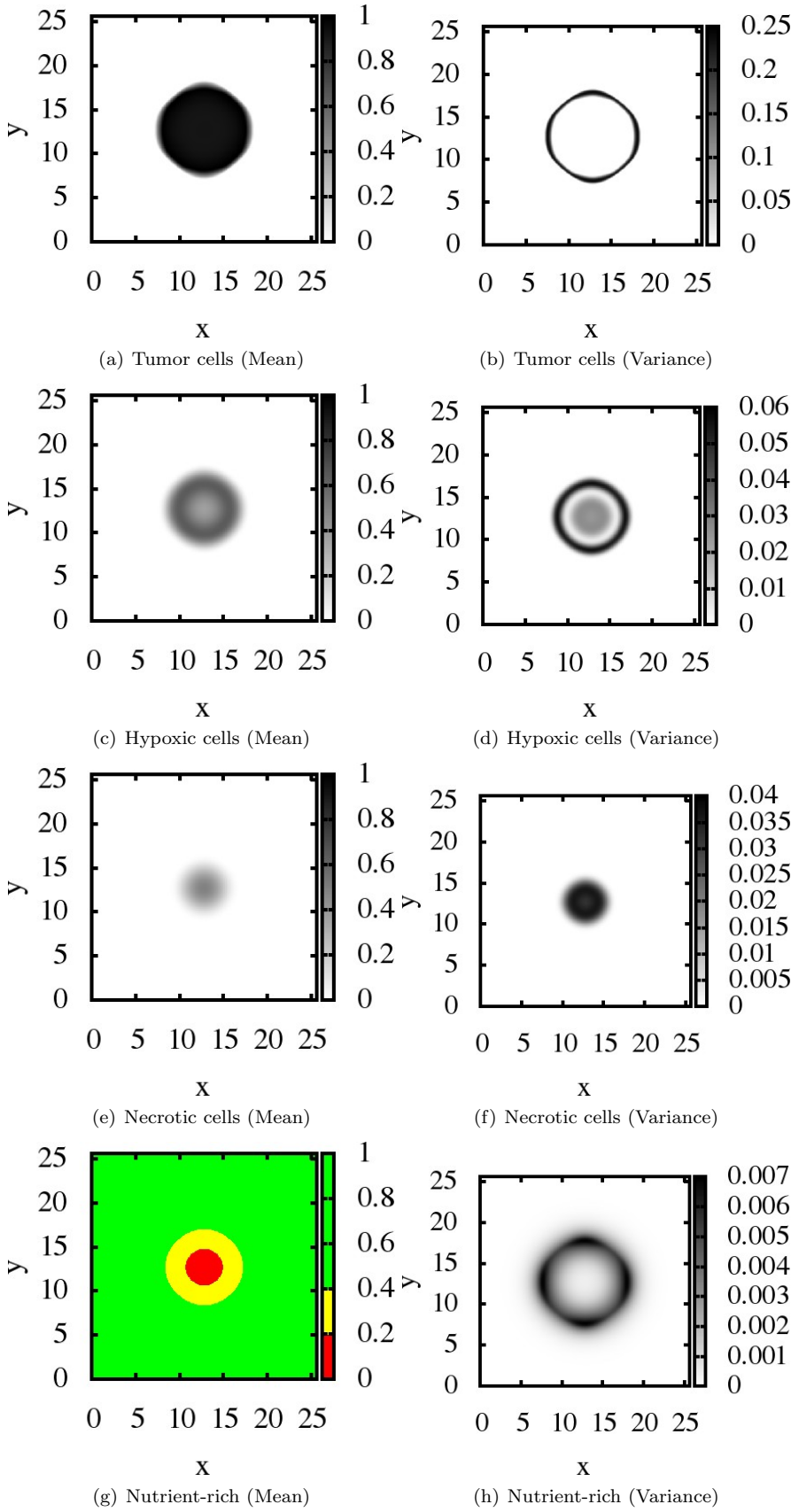

(a) Tumor cells (Mean)

(b) Tumor cells (Variance)

(c) Hypoxic cells (Mean)

(d) Hypoxic cells (Variance)

(e) Necrotic cells (Mean)

(f) Necrotic cells (Variance)

(g) Nutrient-rich (Mean)

(h) Nutrient-rich (Variance)

Figure 5: First row shows the mean values for tumor, hypoxic and necrotic cells and nutrient-rich, second row shows the respectively variance.

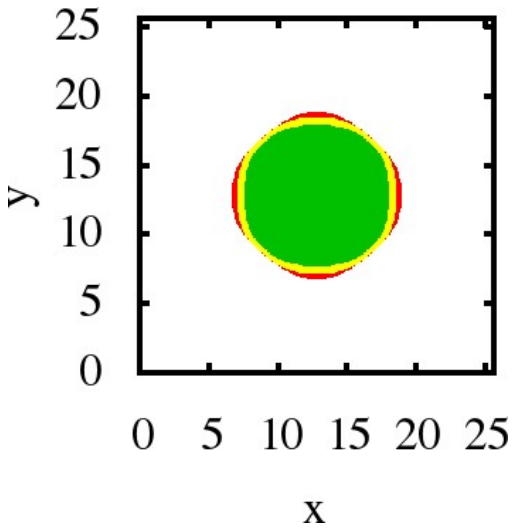

Figure 6: Tumor cells at $t = 10.5$. In yellow the result for the Stochastic Collocation method, in red when $\gamma = 1$ and in green when $\gamma = -1$.

In the next experiment, a different initial configuration of the tumor mass and availability of nutrients is considered over the same computational domain and using the same discretization parmeters as before. The initial tumor mass is composed of three non-connected tumor clusters, as shown in Figure 7(a), defined as

$$\left\{(x,y) : \frac{(x-12.8)^2}{2} + \frac{(y-12.8)^2}{2} \leq 0.32\right\}; \tag{30}$$

$$\left\{(x,y) : \frac{(x-15.36)^2}{2} + \frac{(y-12.8)^2}{2} \leq 0.32\right\}; \tag{31}$$

$$\left\{(x,y) : \frac{(x-15.36)^2}{2} + \frac{(y-10.24)^2}{2} \leq 0.32\right\}. \tag{32}$$

As in the previous experiments, it is assumed that there are sufficient nutrients such that the nutrient concentration is set equal to 1 over the domain. For boundary conditions, we assume that the boundary Γ is divided as shown in Figure 7(b), and we set the following boundary conditions:

$$\boldsymbol{\nabla}\phi_T \cdot \boldsymbol{n} = \boldsymbol{\nabla}\mu \cdot \boldsymbol{n} = \boldsymbol{\nabla}\phi_H \cdot \boldsymbol{n} = \boldsymbol{\nabla}\phi_N \cdot \boldsymbol{n} = 0, \text{on } \Gamma \times (0,T); \tag{33}$$

$$\boldsymbol{\nabla}\phi_\sigma \cdot \boldsymbol{n} = 0, \text{on } E, S \times (0,T); \tag{34}$$

$$\phi_\sigma = 1. \text{on } W, N \times (0,T). \tag{35}$$

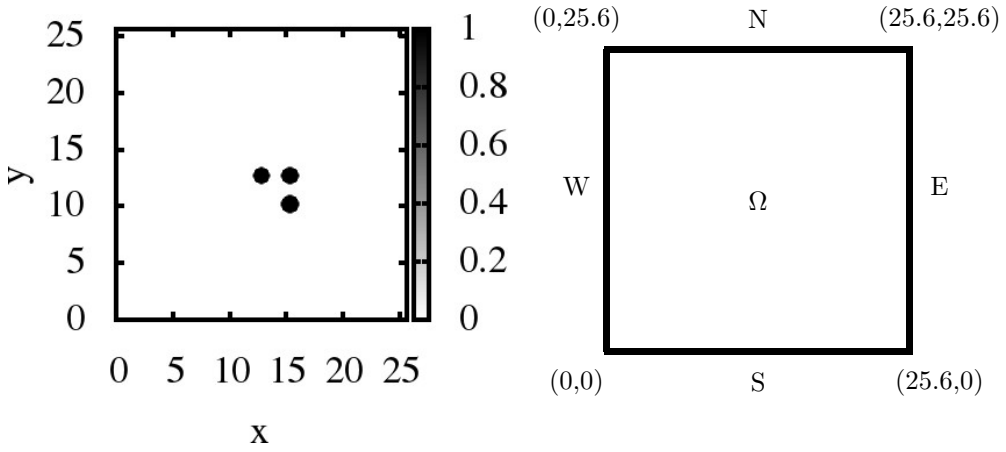

(a) Tumor initial condition (b) Domain representation

Figure 7: New tumor initial condition and domain representation for the second experiment.

To quantify the uncertainty due to a random rate of proliferative cellular mitosis λ_P, we first compare the evolution of the total tumor mass with the two limit cases corresponding to the Worst-Case Scenarios for the rate of proliferative cellular mitosis ($\gamma = -1$ and $\gamma = 1$). Figure 8(a) shows the mean value for the total tumor mass obtained with the Stochastic Collocation method (in red) and with the Worst-Case Scenarios (in blue). At the very beginning, the growth is exponential but is reduced afterwards due to the decrease of nutrient availability. Due to this limitation, the variance of the tumor mass, depicted in Figure 8(b), is zero at the beginning, peaks at $t = 13$, and is reduced afterwards, mainly due to higher concentrations of hypoxic and necrotic cells.

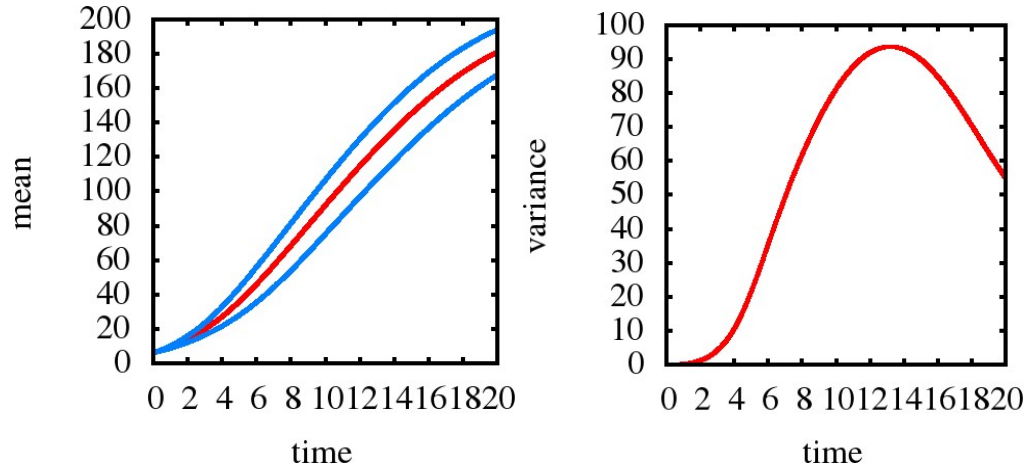

(a) Mass of tumor cells (mean) (b) Variance

Figure 8: Left: mass of the tumor for the random problem in red and in blue the Worst-Case Scenarios. Right: the variance for the mass of the tumor for the random problem.

Figure 9 depicts the mean and variance for the tumor, hypoxic and necrotic cells and nutrient-rich extracellular water at $t = 13$. Figure 9(a), shows that the three initial tumor masses grow independently possibly due to the chemotactic response, that induces the tumor growth towards the higher nutrient concentration. The higher variance of the tumor cells is concentrated mainly on the external diffusive interface of the tumor, where the velocity of the tumor growth changes and where there is more proliferative cells. Similar behavior happens to the variance of the nutrient volume fraction, although there is a decay towards the tumor core due to the presence of hypoxic cells. Finally, in Figure 10 we compare the shapes of the tumor resulting from the random proliferative cellular mitosis (in red) and from using a fixed value for the proliferative cellular mitosis (in green when $\gamma = 0$ - deterministic case). Clearly, the tumor mass is under estimated in

the deterministic case, which can lead to under estimated treatment protocols when planing the action of various therapies, such as chemotherapy.

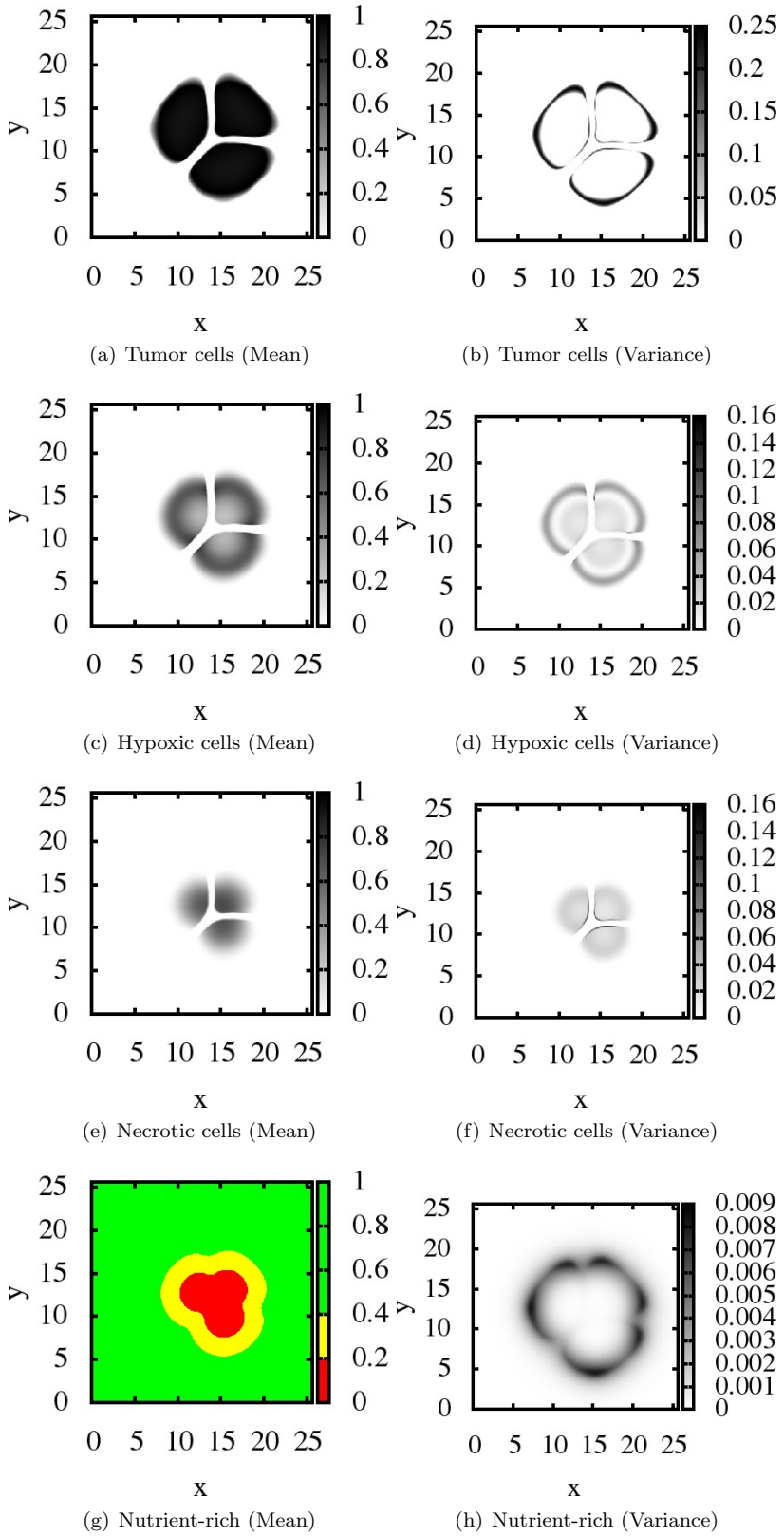

(a) Tumor cells (Mean)

(b) Tumor cells (Variance)

(c) Hypoxic cells (Mean)

(d) Hypoxic cells (Variance)

(e) Necrotic cells (Mean)

(f) Necrotic cells (Variance)

(g) Nutrient-rich (Mean)

(h) Nutrient-rich (Variance)

Figure 9: First row shows the mean values for tumor, hypoxic and necrotic cells and nutrient-rich, second row shows the respectively variance.

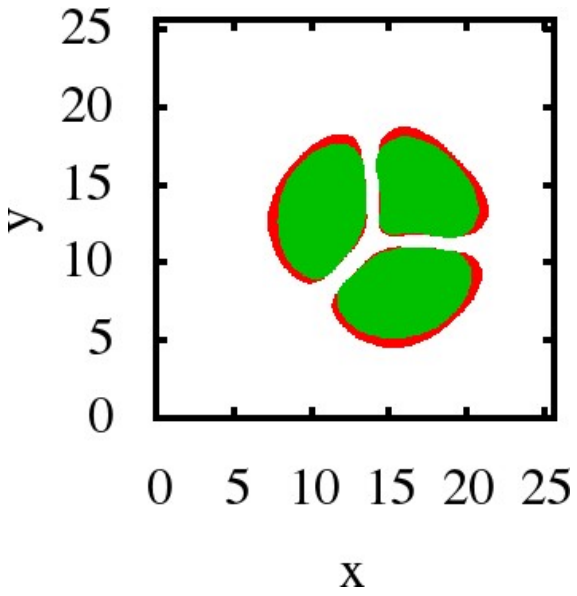

Figure 10: Tumor cells at $t = 13$. In red the mean result for the random problem, in green when $\gamma = 0$.

6. Conclusions

This study describes a general framework for developing and numerically treating a complex stochastic model coming from a multi-species model of tumor growth. We develop a stochastic phase-field model of tumor growth in which the parameters are subjected to uncertainties. The avascular six-species model is a simplification of a previously developed model [13] and considers the interactions of multiple evolving species, such as tumor cells (proliferative, hypoxic and necrotic cells), nutrients and healthy cells. To reduce the number of stochastic parameters and then consider the uncertainty arising just from the most influential parameter, a sensitivity analysis is performed that produces scatterplots of tumor mass versus various model components. The rate of proliferative cellular mitosis is the most influential parameter in the total tumor mass size, followed by the nutrient mobility. The stochastic model is built by considering a continuous uniform distribution for the rate of proliferative cellular mitosis. The resulting system of nonlinear stochastic partial differential equation is then solved through a mixed finite element method and a stochastic collocation scheme for approximating random-variables components of the solution. For the ranges of parameters used here, the inclusion of uncertainty in the rate of proliferative mitosis yields different rates of tumor growth and shapes of the tumor as compared with deterministic experiments and a higher difference (variance) is observed over the interface between tumor and healthy cells. More remarkably, the evolution of the tumor mass is underestimated in the deterministic case. This issue is particularly important when planing the action of various therapies, such as chemotherapy an underestimated tumor mass could lead to insufficient treatment protocols. The extension of these studies to models of angiogenesis and metastasis are targets of future work.

Acknowledgements

The supports of E.A.B.F.L. through Ph.D. Brazilian Fellowship Program CAPES (9141-12-0) and CNPq (140695/2010-9), of J.T.O. by NSF Grant DMS-1115865, and of R.C.A. by CNPq-Brazil (304510/2010-0) are gratefully acknowledged.

7. References

[1] Albano, G. and Giorno, V. A stochastic model in tumor growth. *Journal of Theoretical Biology*, 242(2):329 – 336, 2006.

[2] Albano, G., Giorno, V., Román-Román, P., and Torres-Ruiz, F. Inference on a stochastic two-compartment model in tumor growth. *Computational Statistics and Data Analysis*, 56:1723–1736, 2012.

[3] Andre, N., Barbolosi, D., Billy, F., Chapuisat, G., Hubert, F., Grenier, E., and Rovini, A. Mathematical model of cancer growth controled by metronomic chemotherapies. In *ESAIM: Proceedings*, hal-00751645, November 2012.

[4] Cahn, J. W. and Hilliard, J. E. Free energy of a nonuniform system. I. interfacial free energy. *The Journal of Chemical Physics*, 28:258–267, 1958.
[5] Cristini, V., Li, X., Lowengrub, J. S., and Wise, S. M. Nonlinear simulation of solid tumor growth using a mixture model: invasion and branching. *Journal of Mathematical Biology*, 58:723 – 763, 2009.
[6] Elliot, C. M. The Cahn-Hilliard model for the kinetics of phase separation. In Rodrigues, J. F., editor, *Mathematical models for phase change problems*. Birkhauser, 1989.
[7] Elliott, C. M. and French, D. A. Numerical studies of the Cahn-Hilliard equation for phase separation. *IMA Journal of Applied Mathematics*, 38:97–128, 1987.
[8] Eyre, D. J. Unconditionally gradient stable time marching the Cahn-Hilliard equation. In Bullard, J. W. and Chen, L-Q, editors, *Computational and Mathematical Models of Microstructural Evolution*, volume 529 of *MRS Proceedings*, pages 39–46. Cambridge University Press, November 1998.
[9] Ghanem, R. G. and Spanos, P. D. *Stochastic Finite Elements: a spectral approach, revised Edition*. Dover Publications, Inc., 2003.
[10] Hawkins-Daarud, A., Zee, K. G. Van Der, and Oden, J. T. Numerical simulation of a thermodynamically-consistent four-species tumor growth model. *International Journal for Numerical Methods in Biomedical Engineering*, 8:3 – 24, 2012.
[11] Lamboni, M., Makowski, D., and Monod, H. Multivariate global sensitivity analysis for discrete-time models. *Rapport technique, Unité Mathématiques et Informatique Apploquées, INRA*, (7), 2008.
[12] Le Maître, O. P. and Knio, O. M. *Spectral Methods for Uncertainty Quantification*. Springer, 2010.
[13] Lima, E. A. B. F., Almeida, R. C., and Oden, J. Tinsley. A hybrid ten-species phase-field model of tumor growth. *Mathematical Models and Methods in Applied Sciences*, to appear:1–32, 2014.
[14] Liotta, L. A., Saidel, G. M., and Kleinerman, J. Stochastic model of mestastases formation. *Biometrics*, 32:535–550, 1976.
[15] Lo, C. F. Stochastic Gompertz model of tumour cell growth. *Journal of Theoretical Biology*, 248:317–321, 2007.
[16] Macklin, P., Edgerton, M. E., Thompson, A. M., and Cristini, V. Patient-calibrated agent-based modelling of ductal carcinoma in situ (dcis): From microscopic measurements to macroscopic predictions of clinical progression. *Journal of Theoretical Biology*, 301(0):122 – 140, 2012.
[17] Mallet, D. G. and De Pillis, L. G. A cellular automata model of tumor-immune system interactions. *Journal of Theoretical Biology*, 239:334–350, 2006.
[18] Naumov, L., Hoekstra, A., and Sloot, P. Cellular automata models of tumour natural shrinkage. *Physica A: Statistical Mechanics and its Applications*, 390(12):2283 – 2290, 2011.
[19] Niemisto, A., Dunmire, V., Yli-Harja, O., Zhang, W., and Shmulevich, I. Analysis of angiogenesis using *in vitro* experiments and stochastic growth models. *Physical Review E*, 72, 2005.
[20] Nobile, F., Tempone, R., and Webster, C. G. A sparse grid stochastic collocation method for partial differential equations with random input data. *SIAM Journal on Numerical Analysis*, 46(5):2309–2345, 2008. doi: 10.1137/060663660.
[21] Oden, J. T., Hawkins, A., and Prudhomme, S. General diffuse-interface theories and an approach to predictive tumor growth modeling. *Mathematical Models and Methods in Applied Sciences*, 20(3):477–517, 2010.
[22] Quaranta, V., Weaver, A. M., Cummings, P. T., and Anderson, A. R. A. Mathematical modeling of cancer: The future of prognosis and treatment. *Clinica Chimica Acta*, 357:173–179, 2005.
[23] Saltelli, A., Ratto, M., Andres, T., Campolongo, F., Cariboni, J., Gatelli, D., Saisana, M., and Tarantola, S. *Global Sensitivity Analysis: The Primer*. John Wiley & Sons, 2008.
[24] Tan, W. Y. and Chen, C. W. Stochastic modeling of carcinogenesis: Some new insights. *Mathematical and Computer Modelling*, 28:49–71, 1998.
[25] Wise, S. M., Lowengrub, J. S., Frieboes, H.B., and Cristini, V. Three-dimensional multispecies nonlinear tumor growth - I model and numerical method. *Journal of Theoretical Biology*, 253:524– 543, 2008.
[26] Xiu, D. *Numerical Methods fo stochastic computations: a spectral method approach*. Pinceton University Press, 2010.

Dimensionless parameters

The basic set of parameters values is defined in Table 1. The parameters values are extracted directly from Lima et al. [13], in which both the parameters reported in the literature and those specified on the basis of heuristics connected with our current understanding of certain biological behaviors are listed.

Table 1: Basic set of deterministic parameter values.

Parameter	Value	Meaning	Ref.
$\bar{M}_P$	200	proliferative cells mobility	[10]
$\bar{M}_H$	20	hypoxic cells mobility	[13]
$\bar{M}_N$	0	necrotic cells mobility	[13]
D	1	nutrient mobility	[10]
λ_P	0.5	rate of tumor cellular mitosis	[5]
λ_A	0.0	rate of tumor cellular apoptosis	[5]
λ_{Ph}	0.5	nutrient consumption coefficient by hypoxic cells	[13]
λ_{PH}	0.5	transfer coefficient from ϕ_P to ϕ_H	[13]
λ_{HP}	0.5	transfer coefficient from ϕ_H to ϕ_P	[13]
λ_{HN}	0.5	transfer coefficient from ϕ_H to ϕ_N	[13]
ϵ_T	0.005	interfacial strength among tumor cells and other constituents	[5]
χ_0	0.035	chemotactic constant	[10]
δ_σ	0.01	coefficient that controls the increase of energy due to nutrient	[10]
σ_{PH}	0.4	nutrient threshold involved in the transfer from ϕ_P to ϕ_H	[3]
σ_{HP}	0.5	nutrient threshold involved in the transfer from ϕ_H to ϕ_P	[3]
σ_{HN}	0.3	nutrient threshold involved in the transfer from ϕ_H to ϕ_N	[3]
$\bar{E}$	0.045	energy scale of the bulk energy of tumor cells	[5]